JOURNAL OF CATALYSIS 139, 153–174 (1993)

The Effect of Calcination on H_2 Spillover in Pt/MoO_3

I. Characterization and Kinetics

J.-G. KIM, J. Z. SHYU,[1] AND J. R. REGALBUTO[2]

Department of Chemical Engineering, University of Illinois at Chicago, P.O. Box 4348, Chicago, Illinois 60680

Received October 30, 1991; revised June 9, 1992

The effect of catalyst preparation on the morphology of Pt/MoO_3 and the kinetics of hydrogen spillover have been qualitatively investigated in this first of two works. The morphology of the materials has been characterized by transmission electron microscopy and selective chemisorption, and the chemical state of Pt and the presence of chlorine have been determined with XPS and EDXS. The kinetics of hydrogen spillover in Pt/MoO_3 catalysts as a function of calcination temperature has been recorded with isothermal and temperature programmed reduction experiments. As the calcination temperature of the Pt/MoO_3 samples was increased, the initial rate of reduction (hydrogen uptake) increased and the temperature of initial reduction decreased. Characterization indicates that as calcination temperature is increased, overlayers of MoO_3 on Pt are produced, but additionally the Cl content associated with the Pt phase diminishes. The roles of overlayers and residual chlorine are postulated as follows: overlayers improve the degree of contact of MoO_3 with Pt crystallites, giving hydrogen access to more MoO_3 particles and increasing total H_2 uptake. On the other hand, the intrinsic rate of H_2 spillover from Pt particles into the bulk of MoO_3 appears to be controlled by the amount of residual Cl. When the Pt phase is well dispersed in a series of samples differing only by calcination temperature, it appears that the enhanced H_2 spillover rate stems not from a promotion due to MoO_3 overlayers, but by a lessening of spillover inhibition caused by chlorine.

INTRODUCTION

The phenomenon of hydrogen spillover from a noble metal such as Pt to molybdenum trioxide or its relative, tungsten trioxide, which results in a solid "hydrogen bronze," has been known for quite some time (*1–6*). The process of forward spillover upon exposure of molybdenum trioxide, MoO_3, to elemental hydrogen can be represented as

$$H_2 + MoO_3 \rightarrow H_xMoO_3,$$

where the maximum stable stoichiometry of the molybdenum bronze is $H_{1.6}MoO_3$ (*4*). Pure MoO_3 will not reduce in the presence of elemental hydrogen below 400°C (*4–9*), but in the presence of atomic hydrogen, the reduction can occur at 50°C (*4, 9*). In Pt/MoO_3 mixtures, hydrogen dissociatively adsorbed on Pt can then migrate and "spill over" onto and into the supporting trioxide. Spillover is a reversible process, and noble metal/trioxide catalysts can be exploited to perform reverse spillover reactions such as ethylene hydrogenation (*10*). In more recent studies spillover in Pt/V_2O_5 (*11*) and $Pt/VMoO_{5.5}$ (*12*) systems has been examined.

While it does not influence the final composition of the hydrogen bronzes, the preparation of Pt/transition metal oxide samples greatly influences the rate of hydrogen spillover. On several occasions it has been reported that the calcination of Pt/MoO_3 greatly enhances the rate of hydrogen uptake by the trioxide support, for forward spillover (*3*) and for reverse spillover reactions (*10, 11*). Recent work with the Pt/

[1] Address: Amoco Research Center, P.O. Box 3011, Naperville, IL 60540.

[2] To whom correspondence should be addressed.

0021-9517/93 $5.00

$VMoO_{5.5}$ system has shown that the spillover rate depends strongly on the Pt precursor as well as the calcination treatment employed (*12*); variations in the spillover rate were attributed to differences in final Pt crystallite size.

A number of other factors may be significant, however. It has been demonstrated that physisorbed water or alcohols at the adlineation—the one-dimensional line of contact between the Pt and trioxide phases—assists hydrogen spillover (*1*). Physisorbed water or water formed during the course of reducton might have some effect on the reduction rates. A finding in the genesis of $Pt/WO_3/SiO_2$ catalysts was that WO_3 overlayers form on Pt crystallites during calcination (*13, 14*). MoO_3 overlayers have been reported on Rh in $Rh/MoO_3/Al_2O_3$ catalysts (*15, 16*). Overlayers might act as a sort of solid "spillover bridge" to promote hydrogen spillover.

Another possible factor is residual chlorine. A recent study of Ru/SiO_2 catalysts (*17*) concluded that the amount of residual Cl greatly influences the chemisorptive capacity of Ru for CO, O_2, and especially H_2, which adsorbs dissociatively on Ru. Supporting $PtCl_6$ on SiO_2 increased the temperature at which $PtCl_6$ reduction in H_2 ends from 140 to 190°C (*18*). Thus treatments of $PtCl_6$ impregnated onto MoO_3 at moderate temperature might not serve to remove all chlorine. Residual chlorine from noble metal precursors has been reported to bring into question the characterization and activity measurements in more complicated Ir/TiO_2 (*19*) and Ru/TiO_2 (*20*) systems which exhibit the overlayer or decoration effect. The effects of overlayer formation and residual chlorine can be present simultaneously.

The purpose of the present work is to elucidate the effect of calcination on the morphology and kinetics of hydrogen spillover in Pt/MoO_3 samples. The motivation is twofold; first, it represents a fundamental study of catalyst preparation. In this classic system for the study of hydrogen spillover, two more recently discovered and much discussed phenomena of overlayer formation (strong metal–support interactions) and the effect of residual chlorine are both present and are characterized in some detail. Second, it investigates the practical use of MoO_3 to promote Pt-catalyzed reactions involving the transfer of hydrogen. Molybdenum trioxide has been shown to significantly promote the activity of Pt/SiO_2 for benzene hydrogenation (*21*) (to be published shortly), where the promotional role is thought to involve reverse spillover of hydrogen from MoO_3 to the Pt surface.

The present study has been divided into two parts; in the first, the kinetics of hydrogen spillover in Pt/MoO_3 catalysts as a function of calcination temperature and chemical state has been recorded with isothermal and temperature programmed reduction experiments (ITR and TPR, respectively). The morphology of the materials have been characterized by transmission electron microscopy and selective chemisorption, and the chemical state of Pt and the presence of chlorine have been studied with XPS. In a second paper, characterization and kinetic measurements are synthesized with a simple model of the intrinsic kinetics of these forward spillover experiments (*22*).

EXPERIMENTAL MATERIALS AND METHODS

Ammonium molybdate(VI) tetrahydrate (Aldrich, $(NH_4)_6 \cdot Mo_7O_{24} \cdot 4H_2O$), calcined in a muffle furnace exposed to the atmosphere at 500°C for 2 h, was converted completely to the orthorhombic crystalline phase as verified by X-ray diffraction. The surface area of MoO_3 was estimated by TEM to be approximately 7.3 m^2/g. Pt in the amount of 1 wt% was added by impregnation to incipient wetness of hexachloroplatinic acid. This required 0.25 ml of solution per gram of MoO_3. Chlorine free $(NH_3)_4Pt(OH)_2$ was not used as a precursor, since this material is very hard to reduce, requiring temperatures above 150°C (*23*). The slurry was dried in air for 12 h at 100°C.

The dried catalyst was then ground to a fine powder. For each kinetic run, 300 mg of sample were used.

Ultra high purity gases (Linde) were further purified with a 4-Å molecular sieve for water and residual hydrocarbon and Alltech oxytraps for oxygen. A mass flow controller (Tylan, model RO-28) was used for all gases except oxygen.

The reactor was a pyrex tube (0.55" ID × 10") surrounded by a split tube furnace. The catalyst bed length was approximately 0.5 cm. A Cole–Parmer (Model 2010) temperature controller was used in either isothermal or programmed heating modes. The gas-phase temperature was measured by a thermocouple inside the catalyst bed.

The reactor was run in the recirculation mode with a nominal flow rate of 30 sccm and a recycle ratio of 70. The volume of the reactor and recycle loop was 290 cm^3, measured both statically (filling the system with a known amount of gas and measuring pressure) and dynamically (tracer washout experiments).

The progress of reduction was monitored by continuous analysis of the effluent using a thermal conductivity detector. A mixture of 2 vol% H_2 in N_2 was used for the ITR experiments and 4% H_2 in N_2 was used for TPR. The heating rate for TPR was 0.68°C/min. The pretreatment schedule and experimental program for both experiments were as follows:

(a) N_2 purge at room temperature, 30 sccm, 1 h;
(b) O_2 purge at room temperature, 30 sccm and 1 h;
(c) O_2 calcination at 30 sccm, 1 h at temps of 100, 200, 300, 400, or 500°C;
(d) cooling in N_2 to room temp at 30 sccm and 1 h;
(e) 2% H_2/N_2 for ITR or 4% H_2/N_2 for TPR mixed in recycle loop at 30 sccm (reactor bypassed and left in N_2, heated to reaction temp);
(f) Valve recycle loop through reactor, ITR or TPR run;
(g) He cooling to room temp at 30 sccm, approximately 10 min;
(h) He purge at 30 sccm and 200°C for 2 h;
(i) He cooling to room temp;
(j) CO chemisorption.

After the reduction segment of each experiment the sample was purged in He and a chemisorption measurement was made by the pulse technique. X-ray diffraction showed that some H_2 was lost from the MoO_3 lattice during this last purging step; this was assumed not to effect the CO uptake on the Pt surface. Crystallites sizes were estimated from CO chemisorption for noncalcined and low-temperature calcined samples which exhibited the maximum level of CO chemisorption. A hemispherical geometry was assumed. Crystallite size was not calculated for the samples in which MoO_3 overlayers were thought to occur.

For morphological characterization, a JEOL 100CX was operated at 100 kV in the transmission mode (TEM). The same regions of 1 wt% Pt/MoO_3 samples were photographed before and after a 300 or 400°C calcination, and in some cases again after a reduction in hydrogen according to the TPR protocol. Carbon-substrated gold finder grids (Pelco) were used for the low-temperature calcinations, while substrateless gold grids were used for the higher calcination temperature. To mount the samples, Pt/MoO_3 powder was dispersed in water, into which the grids were dipped. To calcine or reduce a microscope sample, the edges of the microscope grid was sandwiched in a slotted quartz holder to prevent curling, which in turn was held in a stainless-steel mesh basket and lowered onto glass wool inside the reactor. Approximately a half dozen areas of Pt/MoO_3 were imaged for each experiment; areas shown in figures are representative.

The same instrument at 100 kV was used for energy dispersive X-ray spectroscopy (EDXS), to determine the bulk Cl/Pt ratio in Pt crystallites. Spectra were taken of unreduced samples and samples which had

been reduced in a 2% H2 stream for 15 min at 50°C. The spot size was approximately 750 Å. Reported data represents the average measurement of ten separate crystallites, on the order of 200 Å diameter. The Cl/Pt ratio was externally calibrated using solid $PtCl_2$ and $PtCl_4$ compounds deposited onto carbon-substrated grids as solid powders, as well as $PtCl_2$, $PtCl_4$, and $PtCl_6$ compounds which were dissolved in water, deposited onto the carbon substrates, and allowed to dry. The two sets of standards agreed within instrumental error. Care was taken to use a diffuse beam so as to minimize volatilization of $PtCl_x$ compounds (*23*). At typical operating intensity, counting times of 1, 10, 100, and 1000 s with the dissolved $PtCl_2$ standard (containing large $PtCl_x$ crystallites) showed no loss of chlorine. On the other hand, repeated collection times of 100 s (the usual collection time) on small Pt crystallites in $PtCl_x/MoO_3$ samples showed a decrease in the Cl/Pt ratio of about 15%.

All XPS spectra of the catalysts were recorded on a Surface Science SSX-100 XPS spectrometer. Typical operating parameters for the XPS analysis were 600 μ spot size at an analyzer pass energy of 100 eV, which would normally yield a half width of the Au $4f_{7/2}$ of 1.0 eV. A flood gun operated at about 2 eV was used for charge neutralization during analysis. *In situ* XPS runs were performed using a reactor attachment of the spectrometer. A typical flow rate of H_2 used during the pretreatment was 30 ml/min. Fifteen minute isothermal reductions were performed at 50°C. All *in situ* samples were transferred to the analysis changed under UHV to avoid surface reoxidation and contamination.

RESULTS

Morphological Characterization by TEM

The dry impregnation process employed here results in inhomogeneously distributed aggregates of platinum chloride, which do not appear to be strongly bound to the MoO_3 surface. This uneven distribution is seen in Fig. 1, which contains large MoO_3 crystallites and Pt chloride precursors over a carbon film. A relatively dense group of Pt chloride aggregates, which is mainly $PtCl_2$ as seen from the diffraction pattern, had loosened from the MoO_3 surface and deposited onto the carbon film during the TEM sample preparation. Other Pt particles can be seen in relative isolation on MoO_3 crystallites. The amount of beam exposure to these areas was kept very low; it was noted that agglomeration of the precursors occurred upon extended intense beam exposure, behavior which has been reported before for $PtCl_x$ precursors (*24*). Upon calcination at 400°C for 1 h (Fig. 1b), all crystallites shrank in diameter about the same amount as chlorine was released from the aggregates. The average diameter of all crystallites photographed, of which those in Fig. 1b are representative, is approximately 160 Å. Selected area electron diffraction after the calcination step revealed a pattern of fcc (elemental) platinum, with traces of $PtCl_2$.

A 300°C, 1 h calcination in pure O_2 of the Pt aggregate shown in Fig. 2a produced a multiply twinned particle which appeared to be partly covered by an amorphous overlayer, Fig. 2b. In another region, pictured in Fig. 3a, no overlayer structures were apparent after calcination (Fig. 3b). The notable feature here, however, was that considerable swelling or "necking" of the MoO_3 substrate around the base of the Pt particle occurred.

The same type of observations, but more pronounced, occurred upon calcination at 400°C. Pt crystallites became totally covered by amorphous overlayers, as shown in Figs. 4a (before calcination) and 4b (after calcination). The overlayers also appeared on the MoO_3 substrate itself. A different orientation of the sample revealed that swelling of MoO_3 may also have occurred during calcination (Fig. 4c). Shown in Fig. 4d is the same region in the same orientation as Fig. 4c, after a reduction treatment as used in the TPR experiments. Reduction did not significantly change the morphology of the overlayer or Pt crystallite.

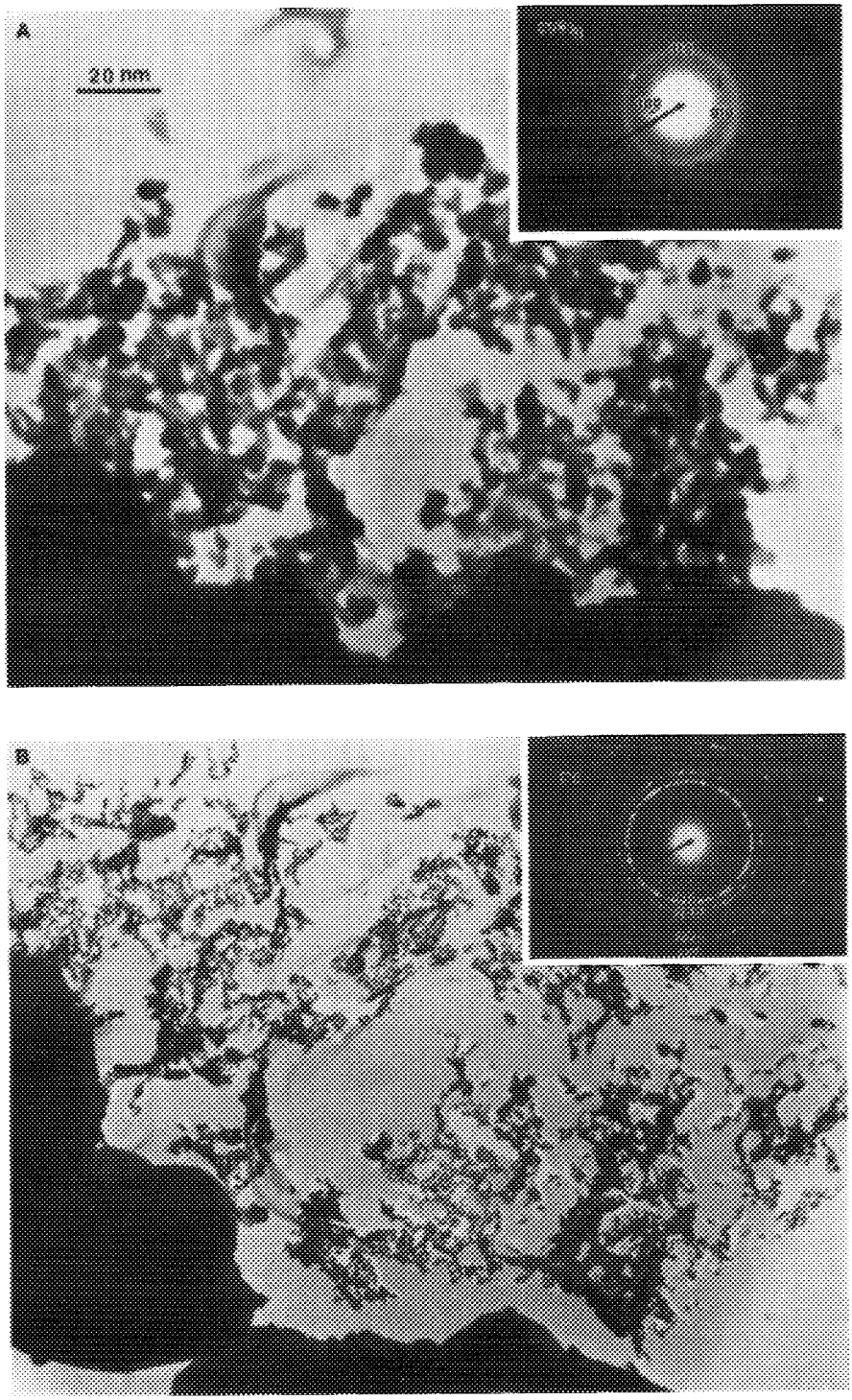

FIG. 1. Distribution of Pt in impregnated 1% Pt/MoO_3 samples (A) before calcination (B) after 400°C calcination in O_2 for 1 h.

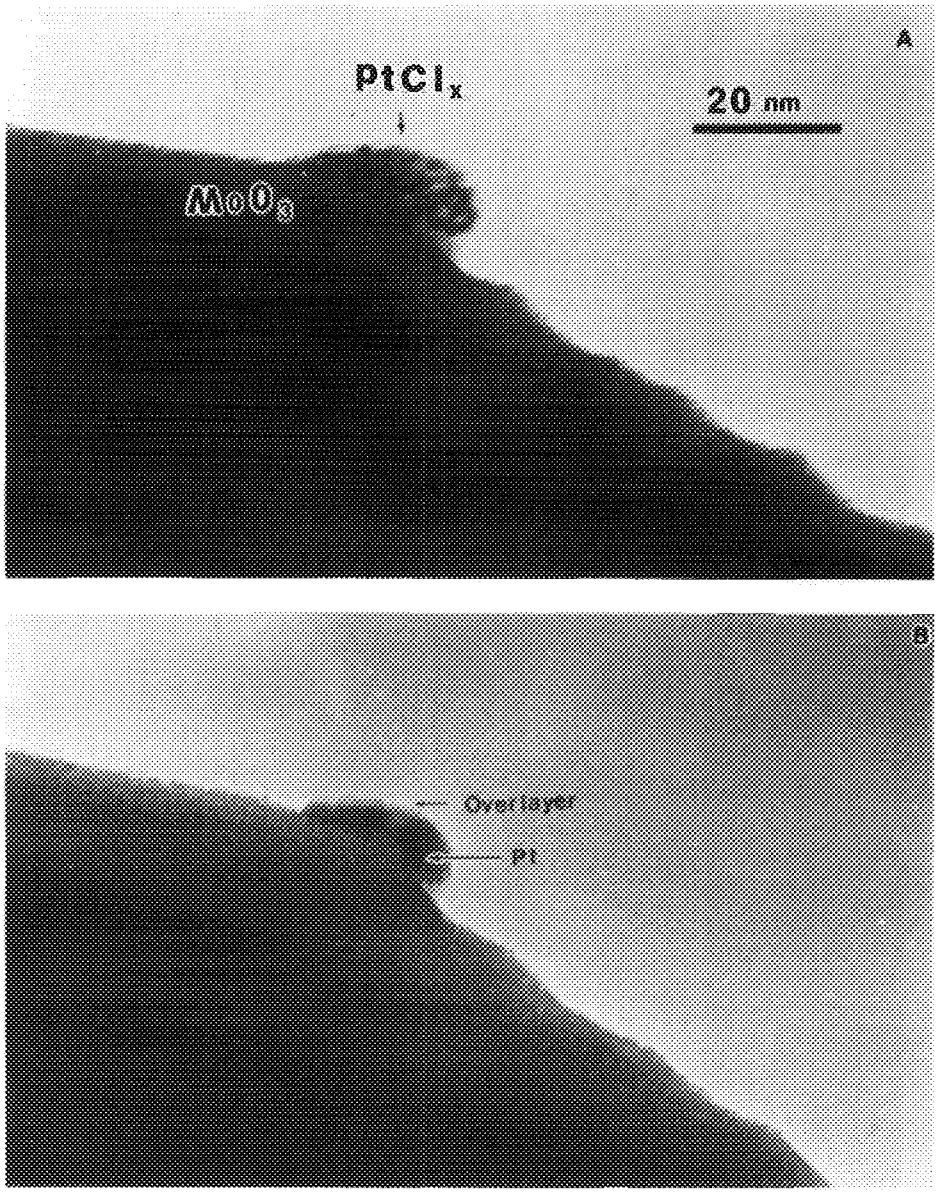

FIG. 2. Effect of 300°C calcination on morphology of 1% Pt/MoO_3: (A) amorphous precursor before calcination; (B) after 300°C calcination in O_2 for 1 h.

For an experimental control, the morphology of just dried and 400°C calcined Pt crystallites supported on silica were studied using nonporous silica spheres of the type employed for model TEM catalyst supports (*25*). Results are shown in Fig. 5; again the grainy, aggregated precursor is seen in Fig. 5a, prior to calcination. The calcination at 400°C results in multiply twinned crystallites, as seen in Fig. 5b. In the dozen or so areas photographed, no evidence of overlayers structures was seen.

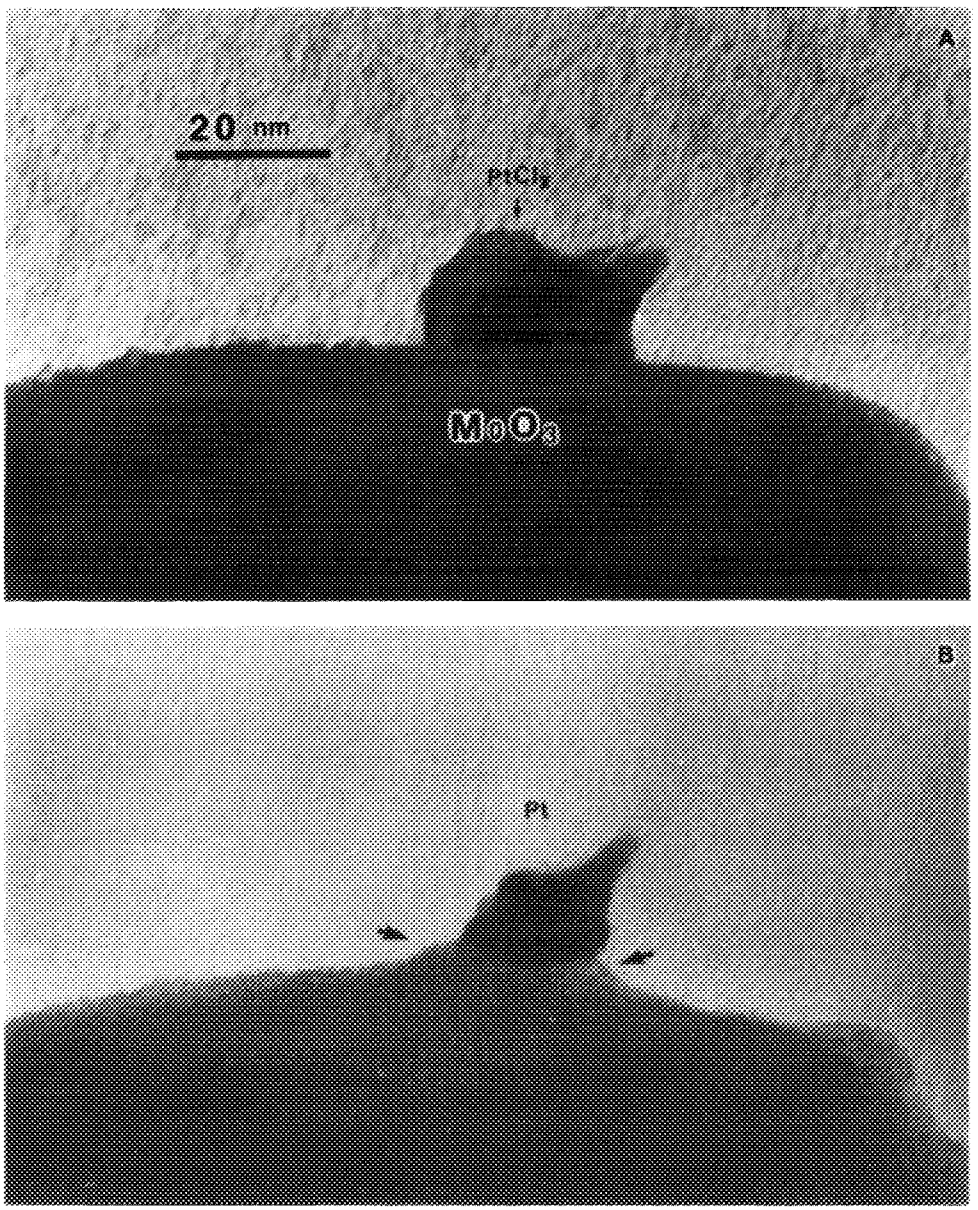

FIG. 3. Effect of 300°C calcination on morphology of 1% Pt/MoO_3: (A) amorphous precursor before calcination; (B) after 300°C calcination in O_2 for 1 h.

Chemical Characterization by XPS and EDXS

To examine the possible influence of the chemical state of Pt and the presence of chlorine on the hydrogen uptake rate, non-calcined and calcined samples were analyzed before and after a 15-min reduction using both XPS and EDXS. The XPS results are shown first. For these experiments, a pure H_2 stream flowing at 30 cc/min was used. Modelling results (*22*) have shown that

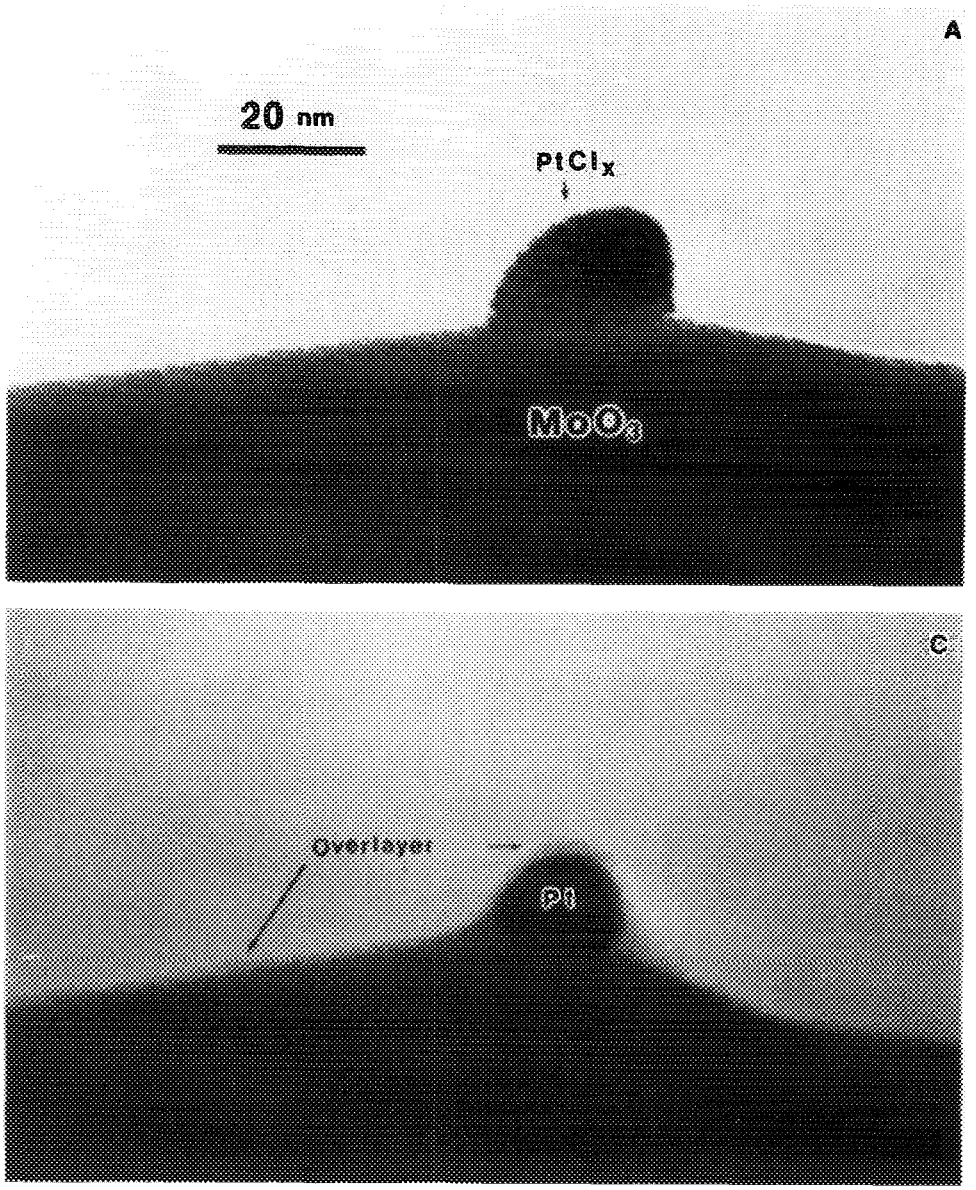

FIG. 4. Effect of 400°C calcination and TPR reduction on morphology of 1% Pt/MoO_3: (A) amorphous precursor before calcination; (B) after 400°C calcination in O_2 for 3 h; (C) rotated approximately 15° with respect to (B); (D) after TPR reduction.

the difference in Pt surface coverage by H_2 at gas concentrations of 2, 4, or 100% is negligible; the rate of $PtCl_x$ reduction in the XPS experiments should be similar to that in the flow experiments. The results are shown in Fig. 6. In Fig. 6a, atomic percents of Mo, Pt, and Cl of the unreduced and reduced samples are plotted as a function of calcination temperature. The balance of the surface is composed of oxygen and carbon (from carbonaceous contamination). As calcination temperature increased, the

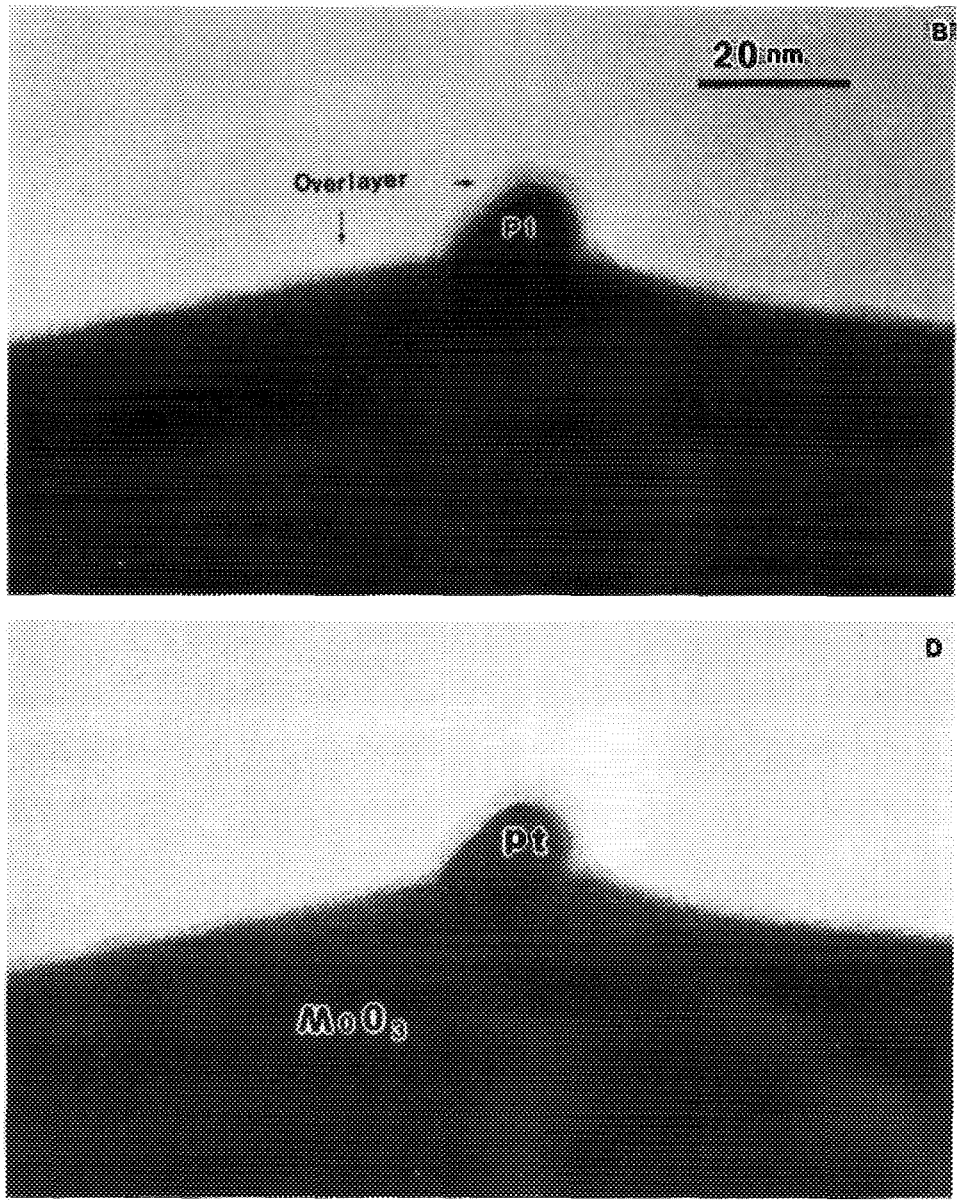

FIG. 4—*Continued*

amount of surface Pt and Cl prior to reduction decreased. The surface composition of Mo varied between 16 and 23 atom%, roughly equal to the bulk composition. Variations in the Mo atom% can be due to different levels of contamination, to the sintering of Pt crystallites, or the disappearance of chlorine. O/Mo and Cl/Pt concentrations are plotted in Fig. 6b. The O/Mo ratios are roughly constant, while the Cl/Pt ratios decrease slowly as calcination temperature is increased. Whereas the measured Cl/Pt ratio increased after reduction of the noncalcined sample from 4.1/1 to 4.7/1, reduction

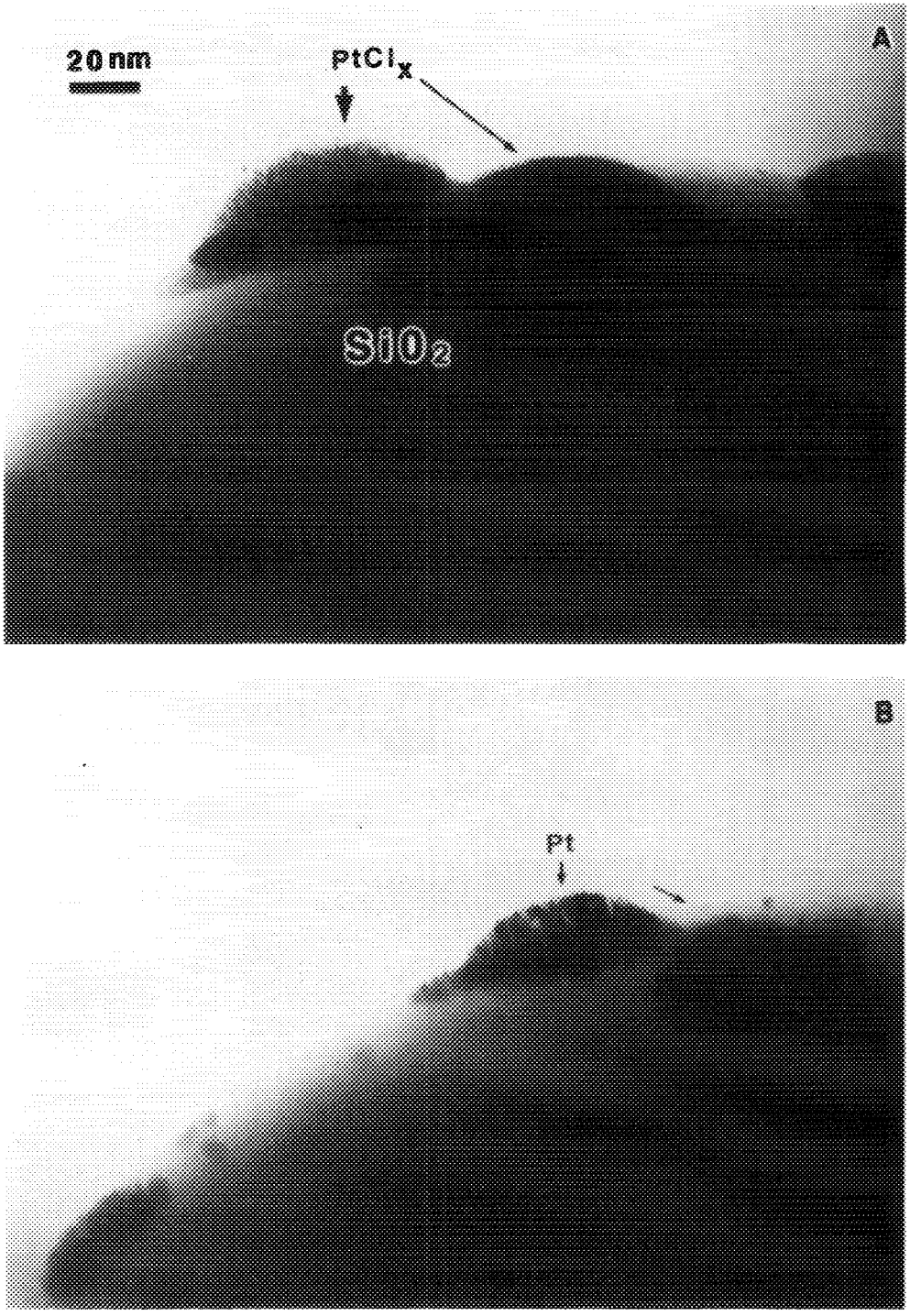

FIG. 5. Effect of calcination on morphology of 0.3% Pt/SiO_2: (A) amorphous precursor before calcination; (B) after 300°C calcination in O_2 for 1 h.

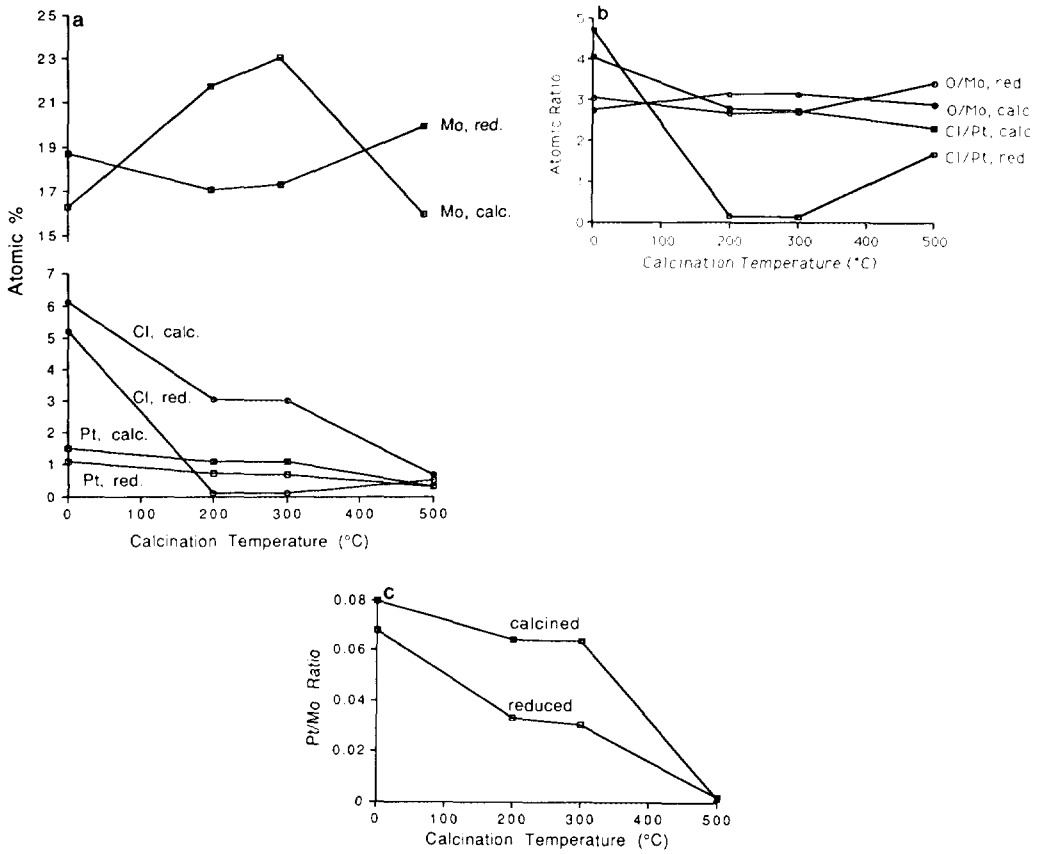

FIG. 6. XPS characterization of H_2 reduction at 50°C: (a) Mo, Cl, and Pt atomic percents before and after reduction; (b) O/Mo and Cl/Pt ratios before and after reduction; (c) Pt/Mo ratios before and after reduction.

of the 200 and 300°C calcined samples brought about a sharp drop in the amount of surface Cl to almost trace levels. The amount of chlorine increased somewhat for the 500°C calcined sample, to a Cl/Pt ratio of 1.6/1. Pt/Mo ratios are shown in Fig. 6c. This ratio decreases as a function of calcination temperature, and also diminishes slightly after the short reduction.

Table 1 summarizes XPS curve fit results for Pt and Mo obtained from a nonlinear least-squares fit. While Pt is present as Pt^{+2} for all samples prior to reduction, Pt in the reduced samples is in both metallic and oxidized forms. The percentage of metallic Pt produced by the reduction appears to increase as the calcination temperature increased, from 43% for the noncalcined sample to 80% for the 500°C calcined sample. A similar trend is seen in the reduction of Mo, which was reduced to a Mo^{+4} species. The degree of reduction in the noncalcined and 200°C calcined samples corresponds to a bronze composition of about $H_{0.8}MoO_3$, while that of the 300 and 500°C calcined samples corresponds to a bronze composition of about $H_{1.2}MoO_3$. This is approximately the same trend as bulk Mo reduction observed with ITR (Table 2).

The Cl/Pt ratio in the bulk of the Pt phase, as determined by EDXS, is plotted in Fig. 7 as a function of calcination temperature.

TABLE 1

XPS Results for 1% Pt/MoO_3

Treatment	Binding energy (eV)[a]			% Red. Pt	% Red. Mo
	Pt4$f_{7/2}$	Pt4$d_{5/2}$	Mo3$d_{5/2}$	Total Pt	Total Mo
Noncalcined					
Before	73.1		233.1		
After	71.5 (43%)[b]		299.9 (38%)[c]	43	38
	72.8 (57%)		231.5 (62%)		
200°C Calcined					
Before		316.7	232.5		
After		314.8 (75%)	230.4 (40%)	75	40
		316.8 (25%)	232.0 (60%)		
300°C Calcined					
Before		316.7	232.5		
After		314.9 (80%)	230.4 (61%)	80	61
		316.4 (20%)	232.7 (39%)		
500°C Calcined					
Before	72.8		232.8		
After	71.1 (80%)		229.9 (57%)	80	57
	73.3 (20%)		231.6 (43%)		

[a] All BEs are referenced to C_{1s} of hydrocarbons at 284.6 eV.
[b] BEs for Pt^0: Pt4$f_{7/2}$ = 71.3 eV, Pt4$d_{5/2}$ = 314.8 eV.
[c] BEs for Mo: 230.0 eV for Mo^{+4}, 232 eV for Mo^{+6}.

The chlorine level in calcined samples is constant and corresponds to $PtCl_6$ until a calcination temperature of 300°C, where about 40% of the Cl is lost. Reduction removes about half of the chlorine in the samples calcined at or below 200°C, while almost all is lost from the 300°C calcined sample.

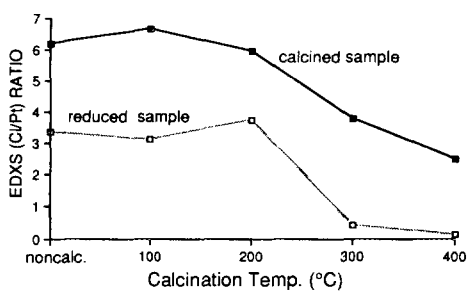

FIG. 7. EDXS characterization of H_2 reduction at 50°C before reduction and after reduction.

Spillover Kinetics and Chemisorption

The hydrogen uptake patterns from a series of Pt/MoO_3 samples subjected to various calcination treatments and reduced isothermally at 50°C is shown in Fig. 8. In this work "reduction" is taken to mean the formation of the hydrogen bronze, which reduces the valence of molybdenum. Post reduction XRD patterns of selected samples were in good agreement with the samples' hydrogen content. The loss of oxygen from the MoO_3 lattice (the formation of water) was never observed. The CO chemisorption results and computed bronze compositions after 240 min are given in Table 2. For the Pt-free sample, CO chemisorption in the amount of 0.5 μl was recorded and no H_2 uptake was observed in the ITR run. The deflection in this pattern is the same as that of an empty reactor. This is due to the filling of the reactor which was bypassed and kept in an inert while a steady-state temperature

TABLE 2

CO and Total H_2 Uptake

Spectrum	Calcination temp. (°C)	ITR CO chem (μl)	Final comp.	TPR CO chem (μl)	Final comp.
(b)	Noncalcined	21.8	$H_{0.90}MoO_3$	23.5	$H_{1.19}MoO_3$
(c)	100	20.4	$H_{1.05}MoO_3$	25.0.	$H_{1.21}MoO_3$
(d)	200	23.3	$H_{1.20}MoO_3$	20.5	$H_{1.16}MoO_3$
(e)	300	23.2	$H_{1.45}MoO_3$	14.2	$H_{1.15}MoO_3$
(f)	400	9.40	$H_{1.36}MoO_3$	10.8	$H_{1.15}MoO_3$
(g)	500	3.36	$H_{1.08}MoO_3$	0.86	$H_{1.15}MoO_3$

and concentration of H_2 in the rest of the flow system was attained.

The Pt containing, noncalcined sample in Fig. 8 exhibited a 15-min induction time, during which the H_2 concentration rose as in the empty reactor experiment. Reduction finally began with a relatively slow rate, bottomed out quickly, and had a long tail. CO chemisorption for this sample was 21.8 μl. The pattern for the 100°C sample also exhibited an induction period, although much shorter than the previous sample. Re-

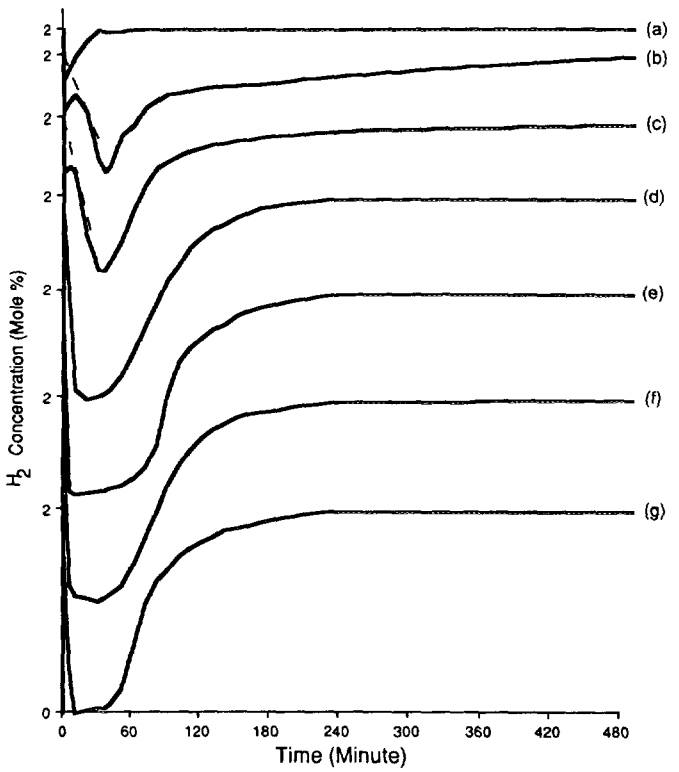

FIG. 8. Isothermal temperature reduction (ITR) experiment at 50°C: (a) empty reactor; (b) noncalcined, calcination at: (c) 100°C, 1 h; (d) 200°C, 1 h; (e) 300°C, 1 h; (f) 400°C, 1 h; (g) 500°C, 1 h. The vertical scale corresponds to 0–2 mol% H_2 concentratoin. Scales for each pattern are offset by arbitrary amounts.

duction occurred faster and to a greater extent. CO chemisorption remained approximately constant. At or above a 200°C calcination, the induction period was no longer evident. Reduction was rapid such that deflections in the various patterns returned to the baseline within at most about 240 min. While CO chemisorption remained about constant for the 200 and 300°C calcined samples, it decreased to 9.4 μl for the 400°C calcined sample and to 3.4 μl for the 500°C sample. The total H_2 uptake (Table 2) was calculated for each sample by computing the area of the pattern and subtracting the amount of H_2 needed to fill the initially empty (inert-filled and bypassed) section of the reactor. This amount is shown in pattern (a) of Fig. 8. The calculation of initial reduction rates for the high-temperature calcined samples is a much more complicated matter, however. The empty reactor deflection cannot properly be simply subtracted from these patterns, since the rapid uptake of hydrogen into the solid (at early times) also affects the rate of accumulation in the gas phase. A detailed intrinsic kinetic study has been made to more properly deconvolute the reactor behavior from the reduction kinetics (*22*); however, for qualitative purposes the above subtraction will be used. Slopes so estimated are shown in Fig. 8 and on all following reduction patterns as appropriate.

Examining the bronze compositions in Table 2, the noncalcined and 100°C calcined samples exhibited the lower hydrogen composition values, due to the slow H_2 uptake rates. The maximum calculated stoichiometry was $H_{1.45}MoO_3$ for the 300°C calcined sample. The 500°C calcined sample exhibited a somewhat lower stoichiometry, even though the ITR pattern returns to the baseline and the reduction appears complete. These compositions were consistent with powder X-ray diffraction patterns of the post reduction samples.

A set of temperature-programmed reduction data for the various calcination temperatures is shown in Fig. 9. The CO chemisorption trend (Table 2) is approximately the same as in the ITR experiments, except that some evidence of overlayer formation is also seen for the 300°C calcined sample. Induction times are again observed in the noncalcined and 100°C calcined samples. Increasing calcination temperature and decreasing CO chemisorption are again associated with an increased initial reduction rate and a decrease in the starting temperature of reduction. It should be noted that reduction for calcinations at 300°C or greater could actually be initiated at subambient temperatures (about −5°C), but due to experimental complications of the cold bath and recycle loop which resulted in poor reproducibility, these experiments are not reported. The shift in starting temperature of reduction is even more drastic than is seen in Fig. 9, however.

The calculated compositions of the hydrogen bronzes formed in the TPR experiments are somewhat lower on average than those of the ITR results and are also in Table 2. This reflects the lower equilibrium composition of the bronzes at the higher final temperature (175°C) of the TPR experiment.

A number of other isothermal reduction experiments were conducted. The H_2 uptake patterns for a calcination temperature of 400°C, with calcination times of 1, 3, and 6 h were virtually equivalent. The shortest calcination time of 1 h yielded the highest CO chemisorption of 9.4 μl. Increasing the calcination time by a factor of 3, CO chemisorption decreased by 28% to 6.8 μl, meaning that overlayer formation on Pt is rather independent of time, and spillover kinetics are rather independent to small changes in the amount of free Pt surface at intermediate values of CO chemisorption.

With extended (2, 4, or 6 h) calcinations at 500°C, chemisorption varied between 0.55 and 2.5 μl. The decrease in CO chemisorption was not always proportional to time and was reproducible only within the range of 0.55–2.5 μl. That is, some of the trials at 6 h exhibited higher CO chemisorption than other trials at 2 h. Repeated trials

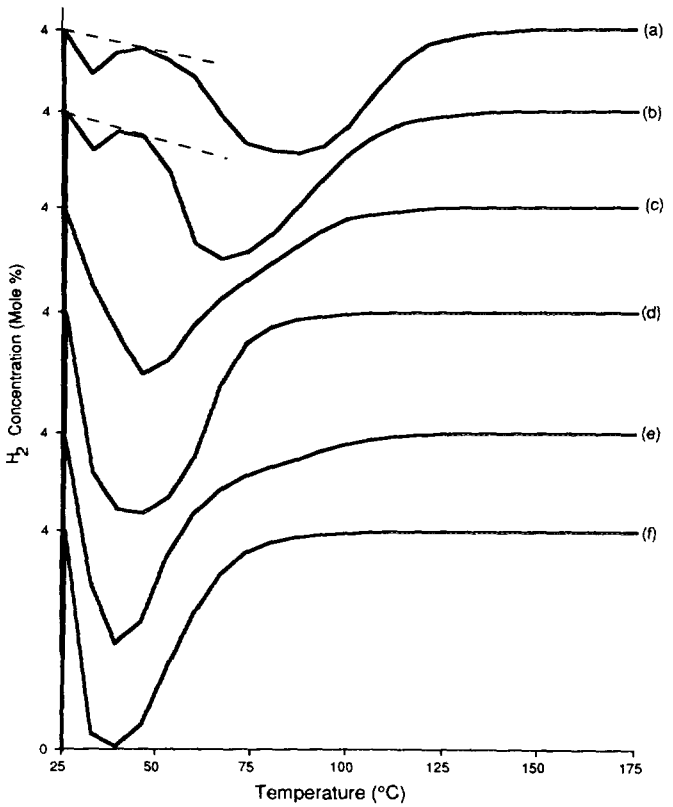

FIG. 9. Temperature programmed reduction (TPR) experiment: (a) noncalcined, and calcination at: (b) 100°C, 1 h; (c) 200°C, 1 h; (d) 300°C, 1 h; (e) 400°C, 1 h; (f) 500°C, 1 h. The vertical scale corresponds to 0–4 mol% H_2 concentration. Scales for each pattern are offset by arbitrary amounts.

at the same temperature were only reproducible within this range. This behavior is thought to arise from the heterogeneity of the samples; all samples may not have contained the large agglomerated deposites of Pt, as shown in Fig. 1. These might not be completely covered by MoO_3 even after long calcination times. In samples where the CO chemisorption was low and approximately equal to MoO_3 itself (0.5 μl), no H_2 uptake was observed. In the samples exhibiting somewhat higher chemisorption (but still below 2.5 μl), the H_2 uptake patterns appeared as in Fig. 8 for the 500°C sample.

To determine if kinetic effects are due to nascent water, two additional samples, noncalcined and 400°C calcined, were reduced isothermally at 110°C. (There has one report of oxygen scavenging from MoO_3 by H_2 in the temperature range 60–110°C (*4*).) Results are shown in Fig. 10 and are qualitatively similar to Fig. 8. The noncalcined sample (CO chemisorption 19.2 μl) exhibits slower H_2 reduction than the 400°C sample (CO chemisorption 6.3 μl). The total amount of H_2 uptaken by the noncalcined sample is somewhat higher than previous, attaining a final composition of $H_{1.14}MoO_3$.

Two final sets of experiments were performed to isolate the potential effects of overlayers and residual chlorine. To isolate the effect of the overlayers, elemental platinum (Pt^0) in the form of Pt black was physically mixed with MoO_3 such that CO chemisorption was about the same as in the noncalcined impregnated sample. Because

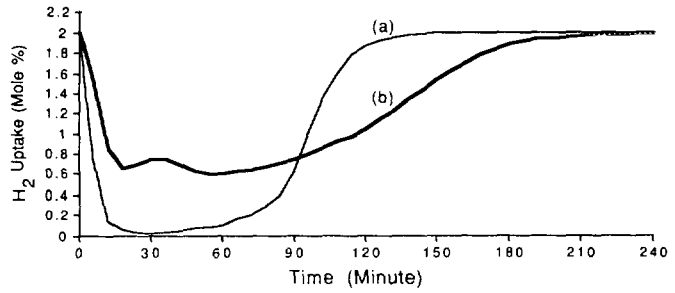

FIG. 10. Isothermal temperature reduction experiment at 110°C: (a) calcination at 400°C, 1 h; (b) noncalcined.

the Pt^0 crystallites were much larger than with the MoO_3 supported crystallites, a Pt loading of 40 wt% was needed to achieve 24.0 μl of CO chemisorption. (As mentioned earlier, ITR was not run with a chlorine-free ammonia Pt precursor since this precursor does not reduce until 150°C (*23*). At this higher temperature oxygen can be lost from the MoO_3 lattice (*4, 5*)). These ITR results at 50°C are seen in Fig. 11, and physical characteristics of the samples are given in Table 3. The top pattern, that of the noncalcined, impregnated H_2PtCl_6 sample, is included for the sake of comparison. With no

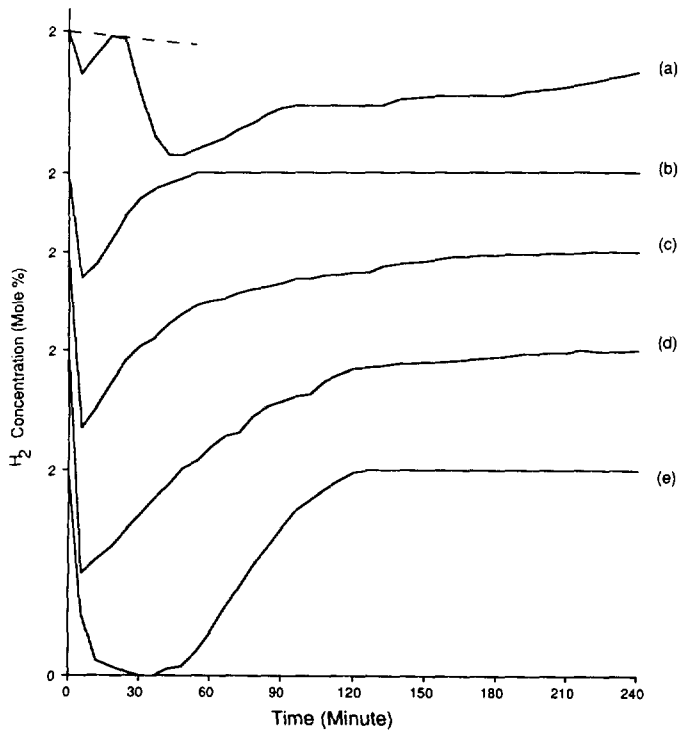

FIG. 11. Pt^0 effect in ITR at 50°C: (a) $H2PtCl_6 \cdot xH_2O$; (b) Pt^0, noncalcined; (c) Pt^0, calcination at 400°C, 1 h; (d) Pt^0, reoxidation at 150°C of (b); (e) Pt^0, 0.06 ml HCl added.

TABLE 3

Characteristics of $Pt^0 + MoO_3$ Physical Mixtures

Spectrum	Sample and pretreatment	wt% Pt	CO uptake (μl)	Calculated cryst. size (Å)	Final comp.
(a)	Impregnated $H_2PtCl_6 \cdot xH_2O$	1.0	24.4	141	$H_{0.90}MoO_3$
(b)	$Pt^0 + MoO_3$ Physical Mix.	40.0	24.0	4600	$H_{0.10}MoO_3$
(c)	$Pt^0 + MoO_3$ calc., 400°C, 1 h	25.0	13.2	Overlayer	$H_{0.53}MoO_3$
(d)	$Pt^0 + MoO_3$, (b) reox., 150°C, 1 h	25.0	9.54	Overlayer	$H_{0.81}MoO_3$
(e)	Pt^0 + HCl	14.3	29.0	1950	$H_{1.04}MoO_3$

calcination of the Pt^0 sample, there is a rapid (no induction time) but small uptake of H_2 (the integrated area of the H_2 pattern is only about twice that for the empty reactor). After a 400°C, 1 h calcination, CO chemisorption dropped to 13.2 μl, which is about the same extent of surface coverage by MoO_3 as seen with the 400°C calcined, impregnated sample. H_2 reduction again proceeds rapidly, and the total uptake increased by a factor of 5 over the noncalcined Pt^0 sample, but was not nearly so high as in the impregnated Pt/MoO_3, 400°C calcined sample in Fig. 8. A pattern similar to the calcined sample (c) was obtained by reoxidizing the reduced Pt^0 sample from pattern (b) for 1 h at 150°C. CO chemisorption of this sample, seen in pattern (d), was slightly lower than in the case of the directly calcined sample (pattern (c)) and the total H_2 uptake was higher by about 53%. Total H_2 uptake was greatly increased by performing an acid impregnation of the $Pt^0 + MoO_3$ mixture, pattern (e). The 14.3 wt% Pt sample resulted in a CO chemisorption of 29.0 μl, about equivalent to the CO chemisorption of the impregnated sample.

A final set of expeirments was conducted with physical mixtures of MoO_3 and different Pt chloride precursors. H_2 ITR patterns at 50°C of these samples are shown in Fig. 12, and their final CO chemisorption, Pt weight loading, and estimated crystallite size from chemisorption are shown in Table 4. The top pattern is again from the impregnated, H_2PtCl_6 sample. The second sample is from a physical mixture of $PtCl_4$ and MoO_3, and the third a mixture of $PtCl_2$ and MoO_3 with roughly the same amount of CO chemisorption (exposed Pt area). The bottom pattern is from a sample containing about twice as much $PtCl_2$ as the previous

TABLE 4

Characteristics of $PtCl_x + MoO_3$, Physical Mixture

Spectrum	Precursor	wt% Pt	CO uptake (μl)	Calculated cryst. size (Å)	Final comp.
(a)	H_2PtCl_6	1.0	24.4	141	$H_{0.90}MoO_3$
(b)	xH_2O	3.10	35.7	313	$H_{1.06}MoO_3$
(c)	$PtCl_4$	8.62	28.4	1150	$H_{1.15}MoO_3$
(d)	$PtCl_2$	18.3	49.3	1660	$H_{1.24}MoO_3$
	$PtCl_2$				

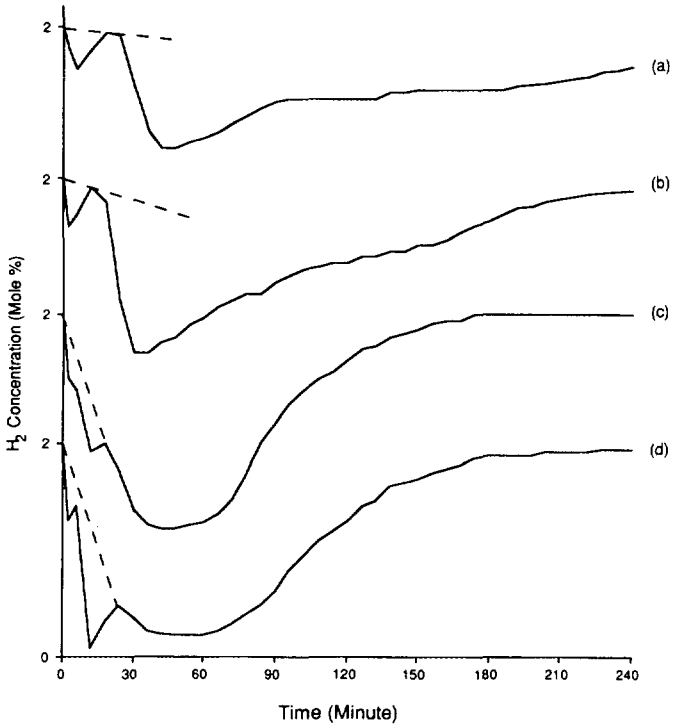

FIG. 12. Chlorine effect in ITR at 50°C: (a) $H_2PtCl_6 \cdot xH_2O$; (b) $PtCl_4$; (c) $PtCl_2$; (d) $PtCl_2$.

sample. From these patterns two observations can be made: the early deflection in the patterns at a time of about 7–20 min is due to the reduction of $PtCl_x$ (the amount of Pt is so low in the samples of Figs. 8 and 9 that this spike is not detected), and second, that the initial rate of reduction increases as the amount of Cl in the precursor is lowered. Appreciable lag times are seen for both the H_2PtCl_6 (pattern a) and $PtCl_4$ (pattern b) samples. The steeper slope of the reduction curve in pattern b, once the reduction begins rapidly, could be attributable to a higher number of Pt perimeter sites (as evidenced in Table 4). The initial slope of the patterns in all cases is less steep than those of the Pt^0 samples in Fig. 11.

DISCUSSION

As the temperature of calcination of the Pt/MoO_3 samples was increased, the rate of hydrogen uptake increased and the temperature of initial reduction decreased. These kinetic observations agree with other comparisons of noncalcined and calcined samples of Pt/MoO_3 (*3*) and $Pt/VMoO_{5.5}$ (*12*) prepared with chloroplatinic acid. As noted in the introduction, at least four factors might account for these trends; the size of Pt crystallites, overlayers of MoO_3 on Pt, physisorbed water or water formed during the course of the experiment, or residual chlorine on Pt. These four possibilities will be examined in the above order.

An estimation of Pt crystallite size from TEM, Figs. 2b–7b, is about 160 Å and agrees well with crystallite sizes calculated from chemisorption results for the noncalcined samples, 158 Å. This would imply that after 240 min of the ITR at 50°C or the TPR, the Pt surface is sufficiently free of Cl, or that Cl does not block H_2 chemisorption on Pt to the extent it does on Ru (*15*). The initially multigrained agglomerates appear

to sinter into one contiguous surface during the 50°C reduction, that is, the Pt crystallites are not of the "snowball" morphology with higher chemisorption area that can be produced with supported rhodium crystallites after oxidation and reduction (*26*). From Figs. 1–5, it is seen that the $PtCl_x$ precursors deposit onto MoO_3 during the drying step in large, isolated agglomerates, and redispersion of these agglomerates does not appear to occur as the result of calcination. Rather, it appears that Pt crystallite size is not significantly affected by calcination temperature. Chemisorption (Table 2) and XPS results (Fig. 6) show that the amount of surface Pt decreases as a function of calcination temperature. Thus, enhanced spillover in Pt/MoO_3 is not due to smaller, better dispersed Pt crystallites as was reported for the $Pt/VMoO_{5.5}$ system (*12*).

Selective chemisorption could be conducted on the Pt/MoO_3 samples, in contrast to $Pt/VMoO_{5.5}$ (*12*), and the decrease in CO chemisorption in the calcined samples can best be explained as blockage of the Pt surface by overlayer formation. The overlayers structures imaged by TEM could not be directly identified by analytical microscopy given their thinness and proximity to Pt. Overlayers are attributed to MoO_3 by comparison to the MoO_3-free Pt/SiO_2 sample, Fig. 5, and in reference to similar claims in the literature for MoO_3 overlayers on Rh in alumina supported catalysts (*15, 16*) and WO_3 decoration of Pt in $Pt/WO_3/SiO_2$ (*13, 14*). The drastic and controlled spreading of MoO_3 on silica during calcination treatments has been well documented (*27, 28*). Like the earlier report on $Pt/WO_3/SiO_2$, overlayers form during the calcination step, and remained relatively unchanged during the reduction step (Fig. 5). This is different from the behavior of materials such as TiO_2 typically associated with decoration effects, in which the mobile species are produced during the reduction step (*29–31*).

XPS results also support the formation of MoO_3 overlayers during calcination. This is evident in Fig. 6c, which shows that the Pt/Mo ratios drops as a function of calcination temperature. A decrease in the Pt/Mo ratio could be due to particle sintering, or to coverage of Pt by MoO_3. Assuming that the Pt crystallite size remains constant and MoO_3 overlayers uniformly cover the Pt surface (which is not actually the case, since CO chemisorption is nonzero for the calcined samples), calculated thickness of MoO_3 on Pt from these ratios are 9.6, 10.7, and 45.4 Å, for the 200, 300 and 500°C calcined samples, respectively. The thickness of overlayers seen by TEM for the 400°C calcination is about 40 Å (Fig. 5).

Even if the existence of MoO_3 overlayers on Pt has been somewhat thoroughly established at this point, the question remains whether they have any role in assisting hydrogen spillover. Two other possible factors are now discussed.

The presence of water could lead to increased H_2 spillover rates, as has been thoroughly demonstrated in the past (*1*); only a small amount of water, present at the small number of $Pt–MoO_3$ adlineation sites, is needed. There are a number of possible sources of water in this experiment. The first is as a significant impurity in the N_2 or H_2 feed gases, however, this would have affected all samples similarly and can be ruled out. A small amount of water might remain physisorbed to the MoO_3 surface through pretreatment, especially in the case of the noncalcined sample; however, the higher calcination temperatures would have removed this and the resulting H_2 uptake would have been slower for the calcined samples. Thus physisorbed water can be ruled out. Third, water might arise from oxygen chemisorbed on elemental platinum produced by the calcination treatments. XPS results, Table 1, show that metallic Pt is present after the calcinations; this would be covered by chemisorbed oxygen. However, the samples exposed to oxygen at 100°C (Figs. 8 and 9) exhibited low H_2 uptake rates, which does not agree with this notion.

Finally, water can be produced from scav-

enging of oxygen from MoO_3 by H_2 (the usual definition of "reduction"), either from bulk crystallites or from overlayers. Most accounts state that this occurs only at or above 200°C, in characterization studies using TGA and DTA (*4*), TGA (*5*), and NMR (*32*) techniques. The lowest claim for O scavenging by H_2 is 60–110°C (*4*), as determined by DTA. The present set of ITR experiments conducted at 110°C (Fig. 10), however, still exhibit the same kinetic trend as the noncalcined and calcined samples reduced at 50°C. The rest of the ITR experiments were conducted at 50°C, and the maximum limit of the TPR experiments was 175°C. There is no indication of water formation at the highest temperatures of the TPR experiment (Fig. 9). Post reaction X-ray diffraction showed no evidence of lower Mo oxides, although this technique could miss a relatively small amount of suboxide.

The remaining possible influence on H_2 spillover rates is the chemical state of the Pt precursor, in particular the presence of chlorine. The amount of surface Cl (from XPS) is shown in Fig. 6, while the amount of Cl in the bulk of the Pt phase (from EDXS) is shown in Fig. 7. The Cl/Pt ratios in Fig. 6c are roughly consistent with the curve fit results for Pt^0 in Table 1. That is, as the Cl/Pt ratio decreases sharply for the 200 and 300°C calcined catalysts, the $\%Pt^0$ increases to 75 and 80% for the two respective samples. However, for the noncalcined sample, the Cl/Pt ratio remains high after the reduction while 43% of the Pt is present as Pt^0. Furthermore, EDXS shows that the bulk of the noncalcined sample is about half reduced by the 15-min reduction. These results suggest that Cl could be present in some residual form, dispersed onto the MoO_3 or Pt surface, possibly blocking the Pt–MoO_3 adlineation. This chlorine could be responsible for slowing the rate of hydrogen transfer from the metallic Pt surface to MoO_3.

The 200°C calcined sample is again about half reduced in the bulk, but the surface is virtually free of Cl in the reduced state. The reduced 300°C calcined sample is almost free from chlorine in both the bulk and on the surface. It appears that after the higher calcinations, at or in excess of 300°C, the remaining $PtCl_x$ phase becomes much easier to reduce. Perhaps the $PtCl_x$ phase formed at these higher temperatures, already partly decomposed as seen in Fig. 7, is more ordered or open, such that the lattice can be more easily penetrated by hydrogen, or more easily negotiated by volatile chlorine species. While this ordering might not be sufficient in the bulk at 200°C, so that the bulk retains relatively high amounts of Cl (Fig. 7), the effect is manifested at the surface such that the surface of the 200°C calcined sample is free of chlorine (Fig. 6).

The effects of residual chlorine versus MoO_3 overlayers are now discussed. Most significantly, the XPS trend of post reduction chlorine (Figs. 6a and 6b) corresponds to the kinetic trends in the ITR and TPR experiments of Figs. 8 and 9 more closely than does the trend in overlayer formation as observed by TEM. That is, the greatest change in H_2 uptake rate occurs between calcination temperatures of 100 and 200°C, with the rate of the 200°C calcined sample almost equal to that of the 300°C calcined sample. Figure 6 shows that the final Cl surface concentration in the 200°C sample is as low as that of the 300°C calcined sample. TEM and chemisorption trends indicate that overlayers do not form until 300 or 400°C, although perhaps some necking of MoO_3 to Pt (Figs. 3b and 5b) could lead to enhanced Pt–MoO_3 contact at lower temperatures.

A comparison of the effects of chlorine and overlayers can be made in light of the ITR and TPR kinetic experiments in Figs. 11 and 12. The effect of chlorine is clearly seen in Fig. 12, in which decreasing the amount of chlorine in the precursor brings about more rapid initial reduction rates. Furthermore, the steepest initial slopes of H_2 reduction are recorded for the chlorine free Pt^0 samples in Fig. 11. Also seen in Fig. 11, it is the total amount of H_2 uptake and not the initial reduction rate that is influenced by

calcination. In the noncalcined Pt^0 sample small total H_2 uptake is expected; the Pt^0 particles are very much larger than those of the impregnated samples, so for the same Pt free surface area there is much less perimeter in contact with MoO_3. Also, less total MoO_3 particles are contacted. The effect of calcination in Fig. 11, whether by an initial 1-h calcination at 400°C or a reoxidation for 1 h at 150°C, is to enhance the degree of Pt–MoO_3 contact, though at the sacrifice of some exposed Pt surface. More total H_2 uptake can occur, but at the same rate as previously. The adsorption rate of H_2 onto Pt is so high that loss of Pt surface is not detrimental, except at extensive levels of overlayer formation. As noted for the 500°C calcined samples calcined for longer times, very extensive overlayer growth can shut off CO chemisorption and H_2 uptake completely.

According to this hypothesis, the lower H_2 composition of the 500°C calcined sample in Fig. 8 is likely due to a portion of the MoO_3 particles being isolated by complete coverage of the Pt particles on them. (Completely covered Pt particles also explains why some chlorine is still observed by XPS for the 500°C calcined sample, in Fig. 6). The higher total uptake of the acid impregnation of the Pt^0 sample in Fig. 12 could be due to dissolution and redispersion of Pt, indicated by the chemisorption results. The initial reduction rate is noticeably slower than those for the Pt^0 samples, which would be due to the presence of chlorine.

From these qualitative arguments the roles of overlayers and residual chlorine are postulated as follows: overlayers improve the degree of contact of MoO_3 with Pt crystallites, giving hydrogen access to more MoO_3 particles and increasing total H_2 uptake. Moderate levels of coverage of the Pt surface are not detrimental, since the net rate of H_2 adsorption on Pt is much faster than the loss of H_2 from the Pt surface by spillover. However, extensive overlayer formation can completely cover Pt particles and so isolate MoO_3 particles from hydrogen. On the other hand, the intrinsic rate of H_2 spillover from Pt particles into the bulk of MoO_3 appears to be controlled by the amount of residual Cl associated with the Pt particles. When the Pt phase is well dispersed in a series of samples calcined at different temperatures, the predominant differentiating factor in the formation of the bronze would be residual chlorine. The enhanced H_2 spillover rates in these calcined samples stems not from a promotion due to MoO_3 overlayers, but by a lessening of the inhibition caused by chlorine. It appears that calcination results in a $PtCl_x$ precursor phase which is more readily reduced than the noncalcined precursor phase. Some detailed suggestions as to the nature of the spillover mechanism in these samples are provided in the following modelling work (*22*).

ACKNOWLEDGMENTS

The support of the Amoco Corporation and the Illinois Department of Commerce and Community Affairs for the completion of this work is gratefully acknowledged.

REFERENCES

1. Benson, J. E., Kohn, H. W., and Boudart, M. *J. Catal.* **5,** 307 (1966).
2. Boudart, M., Vannice, M. A., and Benson, J. E., *Z. Phys. Chem. Ne. Folg. Bd.* **64,** 171 (1969).
3. Tinet, D., and Fripiat, J. J., *J. Chim. Phys. Phys. Chim. Biol.* **76,** 867 (1979).
4. Sermon, P. A., and Bond, G. C., *J. Chem. Soc. Faraday Trans. 1* **72,** 730 (1976).
5. Bond, G. C., and Tripathi, J. B. P., *J. Less-Common Met.* **36,** 31, 1974.
6. Bond, G. C., and Tripathi, J. B. P., *J. Chem. Soc. Faraday Trans. 1* **72,** 933 (1976).
7. Sardi, A., *Acta Chim. Acad. Sci. Hung.* **39,** 145 (1963).
8. Hawkins, D. T., and Worrel, W. L., *Metall. Trans.* **1,** 271 (1970).
9. Fleisch, T. H., and Mains, G. J., *J. Chem. Phys.* **76,** 780 (1982).
10. Marcq, J. P., Wispenninckx, X., Poncelet, G., Keravis, D., and Fripiat, J. J., *J. Catal.* **73,** 309 (1982).
11. Marcq, J. P., Poncelet, G., and Fripiat, J. J. *J. Catal.* **87,** 339 (1984).
12. Lin, X., Francois, J., Lambert, H., and Fripiat, J. J., *Catal. Lett.* **3,** 169 (1989).

13. Regalbuto, J. R., Fleisch, T. H., and Wolf, E. E., *J. Catal.* **107,** 114 (1987).
14. Regalbuto, J. R., Allen, C. W., and Wolf, E. E., *J. Catal.* **108,** 304 (1987).
15. Kip, B. J., von Wolput, J., Hermans, N., van Grondelle, J., and Prins, R., *Appl. Catal.* **35,** 109 (1987).
16. Van der Berg, F., Clezer, J., and Satchler, W. H., *J. Catal.* **93,** 340 (1985).
17. Narita, T., Miura, H., Sugiyama, K., Matsuda, T., and Gonzalez, R. D., *J. Catal.* **103,** 492 (1987).
18. Rejai, B., and Gonzalez, R. D., *J. Catal.* **123,** 113 (1990).
19. Tiep, L. V., Che, M., Bugli, G., and Bond, G. C., *J. Catal.* **99,** 449 (1986).
20. Bond, G. C., and Rajaram, R. R., *Appl. Catal.* **27,** 379 (1986).
21. Kim, J.-G., and Regalbuto, J. R., in preparation.
22. Kim, J.-G., and Regalbuto, J. R., *J. Catal.* **139,** 175 (1993).
23. Hurst, N. W., Gentry, S. J., Jones, A., and McNicol, B. D., *Catal. Rev.-Sci. Eng.* **24,** 233 (1982).
24. Foger, K., and Jaeger, H., *J. Catal.* **92,** 64 (1985).
25. Datye, A. K., and Long, N. J., *Ultramicroscopy* **25,** 203 (1988).
26. Burkhead, J., and Schmidt, L. D., *J. Catal.* **116,** 240 (1989).
27. Datta, A. K., Ha, J.-W., and Regalbuto, J. R., *J. Catal.* **133,** 55 (1992).
28. Datta, A., and Regalbuto, J. R., *Ultramicroscopy* **29,** 233 (1989).
29. Tauster, S. J., *Am. Chem. Soc. Symp. Ser.* **298,** 1 (1986).
30. Logan, A. D., Braunschweig, E. J., Datye, A. K., and Smith, D. J., *Langmuir* **4,** 827 (1988).
31. Dumesic, J. A., Stevenson, S. A., Sherwood, R. D., and Baker, R. T. K., *J. Catal.* **61,** 378 (1980).
32. Cirillo, A., and Fripiat, J. J., *J. Phys.* **39,** 247 (1978).